NEUROSCIENCE
RESEARCH ARTICLE

M. J. Trujillo et al. / Neuroscience 523 (2023) 91–104

# Plasticity of Cortico-striatal Neurons of the Caudal Anterior Cingulate Cortex During Experimental Neuropathic Pain

**María Jesús Trujillo, Constanza Ilarraz and Fernando Kasanetz***

*Universidad de Buenos Aires, Facultad de Ciencias Médicas, Departamento de Ciencias Fisiológicas, Grupo de Neurociencia de Sistemas, Buenos Aires, Argentina*

*CONICET - Universidad de Buenos Aires, Instituto de Fisiología y Biofísica Bernardo Houssay (IFIBIO Houssay), Buenos Aires, Argentina*

**Abstract—Maladaptive neuronal plasticity is a main mechanism for the development and maintenance of pathological pain. Affective, motivational and cognitive deficits that are comorbid with pain involve cellular and synaptic modifications in the anterior cingulate cortex (ACC), a major brain mediator of pain perception. Here we use a model of neuropathic pain (NP) in male mice and ex-vivo electrophysiology to investigate whether layer 5 caudal ACC (cACC) neurons projecting to the dorsomedial striatum (DMS), a critical region for motivational regulation of behavior, are involved in aberrant neuronal plasticity. We found that while the intrinsic excitability of cortico-striatal cACC neurons (cACC-CS) was preserved in NP animals, excitatory postsynaptic potentials (EPSP) induced after stimulation of distal inputs were enlarged. The highest synaptic responses were evident both after single stimuli and in each of the EPSP that compose responses to trains of stimuli, and were accompanied by increased synaptically-driven action potentials. EPSP temporal summation was intact in ACC-CS neurons from NP mice, suggesting that the plastic changes were not due to alterations in dendritic integration but rather through synaptic mechanisms. These results demonstrate for the first time that NP affects cACC neurons that project to the DMS and reinforce the notion that maladaptive plasticity of the cortico-striatal pathway may be a key factor in sustaining pathological pain.**

**Key words: neuropathic pain, anterior cingulate cortex, neuronal plasticity, dorsomedial striatum, corticostriatal neurons.**

## INTRODUCTION

Neuropathic pain (NP) is a highly prevalent and debilitating clinical condition. A large proportion of people suffering from pathological pain are dissatisfied with their treatment (Breivik et al., 2006; Johannes et al., 2010). Therefore, a central goal of current research on pain is to understand the neural mechanisms involved in pathological pain and to identify possible therapeutic targets (Price et al., 2018).

On the cellular level, long lasting consequences of NP are induced by aberrant neuronal plasticity at all stages along the nociceptive pathway, including brain regions involved in pain perception (Costigan et al., 2009; Bliss et al., 2016; Kuner and Flor, 2017) In particular, it is believed that the sensory, emotional, and cognitive consequences of pathological pain and the impaired top-down modulation of pain may be due in part to adaptations in brain neural circuits that mediates those aspects of the pain experience and that participate of the descending control of pain by psychological factors (Bushnell et al., 2013; Baliki and Apkarian, 2015). In support of this, animal models of neuropathic and inflammatory pain are associated with cellular and synaptic alterations in brain structures that mediate motivation, reward, aversion and cognition, such as medial prefrontal cortices (Li et al., 2010; Blom et al., 2014; Cordeiro Matos et al., 2015; Koga et al., 2015; Santello and Nevian, 2015; Lançon et al., 2021), the ventral tegmental area (Ren et al., 2015; Watanabe et al., 2018; Huang et al., 2020) and the basal ganglia (Goffer et al., 2013; Schwartz et al., 2014; Ren et al., 2015).

Human and animal studies implicate the anterior cingulate cortex (ACC) as a central hub for the affective, motivational and cognitive aspects of pain perception in health and disease. Functional imaging in humans showed a significant correlation between ACC activation and the perceived intensity and discomfort produced by noxious stimuli (Tölle et al., 1999; Büchel et al., 2002). People suffering from chronic pain show elevated neural

*Correspondence to: Fernando Kasanetz, Instituto de Fisiología y Biofísica Bernardo Houssay (IFIBIO-Houssay), Grupo de Neurociencia de Sistemas, Facultad de Ciencias Médicas, Universidad de Buenos Aires, Paraguay street 2155, 7th floor, C1121ABG Buenos Aires, Argentina.
E-mail addresses: fkasanetz@fmed.uba.ar, ferkasa@gmail.com (F. Kasanetz).

*Abbreviations:* ACC, anterior cingulate cortex; cACC, caudal ACC; DMS, dorsomedial striatum; EPSP, excitatory postsynaptic potentials; NP, neuropathic pain.

https://doi.org/10.1016/j.neuroscience.2023.05.017
0306-4522/

responses to pain in the ACC associated with an increase in unpleasant sensations (Derbyshire et al., 2002), while patients with lesions or surgical ablation of the ACC presented altered emotional responses to pain (Ballantine et al., 1967; Berthier et al., 1988). Studies in rodents have demonstrated the instrumental role of the ACC in pain sensitivity and aversion, and suggest that different subregions within the ACC may process distinct aspects of the pain experience. Thus, manipulations that reduce or eliminate activity in the rostral part of the ACC (rACC, perigenual areas 24b, portions of perigenual 24a and caudodorsal area 32) impaired aversive responses to noxious stimuli in naif and NP animals (Johansen et al., 2001; Johansen and Fields, 2004; Zhang et al., 2017), while interfering with the activity of the caudal region of the ACC (cACC, postgenual areas 24a and 24b) modulated aversion to pain in NP, but not in intact, animals (LaBuda and Fuchs, 2000; Johansen et al., 2001; LaGraize et al., 2004; Santello et al., 2017; Lançon et al., 2021).

Animal models of pathological pain support the notion that both rACC and cACC are hyperactive upon pathological pain (Zhang et al., 2017; Sellmeijer et al., 2018; Zhao et al., 2018; Zhou et al., 2018; Kasanetz and Nevian, 2021). In this line, inhibition of rACC firing by optogenetic or pharmacological techniques reversed the enhanced aversion induced by noxious stimuli in neuropathic rats (Zhang et al., 2017; Zhou et al., 2018). Interestingly, neuronal activation in the rACC measured with the genetic marker C-Fos showed time-dependent bidirectional changes during chronic facial inflammatory pain in rats (Ducret et al., 2022), suggesting that pathological pain mechanisms in the ACC may be dynamic and that hyperactivity and hypoactivity might concomitantly interact in the different subregions of the ACC.

Diverse neuronal plasticity mechanisms are at the origin of cACC hyperactivity during pathological pain. This comprise increased synaptic transmission onto pyramidal neurons of layers 2/3 (Li et al., 2010; Koga et al., 2015), changes in intrinsic excitability of layer 5 neurons and loss of reciprocal connections between pyramidal neurons and inhibitory interneurons of deep layers of the cACC (Blom et al., 2014; Santello and Nevian, 2015). Notably, these studies also demonstrated that neuronal plasticity in the cACC is required for the expression of the sensory, emotional and affective symptoms of the pathology (Koga et al., 2015; Santello and Nevian, 2015; Santello et al., 2017; Lançon et al., 2021; Li et al., 2021, 2010).

A key integration node between the nociceptive and motivational systems occurs at the level of the medial striatum, where afferents from the ACC converge along with projections from the cerebral amygdala, thalamus, hippocampus, and mesencephalic dopaminergic system (Hunnicutt et al., 2016). Medial and ventral striatal neurons mediate motivation, reward and aversion (Kravitz and Kreitzer, 2012) and their activity in humans correlates with the subjective experience of pain (Scott et al., 2006). Likewise, the functional connectivity between the cerebral cortex and the ventral striatum predicts the persistence of pain in patients (Baliki et al., 2012), suggesting that cortico-striatal transmission is causally involved in the chronification of pain. Moreover, it was recently shown that optogenetic activation of cACC terminals in the dorsomedial striatum (DMS) decreased mechanical and thermal nociceptive thresholds, whereas the inhibition of this pathway relieved hyperalgesia in a mice model of NP (Zhuang et al., 2019), and that projections from the rACC to the nucleus accumbens contributes to NP-induced aversion (Gao et al., 2020).

Taken together, this evidence posits the ACC-corticostriatal (ACC-CS) pathway as a central mediator in the manifestation of acute and pathological pain. Despite this, and considering the importance of neuronal plasticity in the ACC for the manifestation of pathological pain, little is known about how NP alter the functional properties of ACC-CS neurons.

Here we performed patch clamp electrophysiological recording in brain slices to investigate the neuronal plasticity of caudal ACC-CS neurons in a mice model of sciatic nerve injury. We uncovered the functional changes that could facilitate the propagation of corticolimbic abnormal activity to the basal ganglia during pathological pain.

## EXPERIMENTAL PROCEDURES

### Animals

Animals were cared for in accordance with institutional (CICUAL, Faculty of Medicine, University of Buenos Aires) and government regulations (SENASA, Argentina). Male C57/BL6 mice were group-housed, maintained in 12-h light/dark cycles and had unrestricted access to food and water. For identification, small holes were punched into the mouse ears.

### Viral vectors injection

In order to identify cortico-striatal ACC neurons, we injected in the DMS an adenoviral vector for retrograde infection expressing the fluorescent tag EGFP or mCherry (AAV-retro/2-hSyn1-chI-EGFP-WPRE-SV40p or AAV-retro/2-hSyn1-chI-mCherry-WPRE-SV40p; Viral Vector Facility, University of Zurich). Viral vectors were aliquoted and stored at −80 °C until the day of surgery, when were diluted 1:2 in PBS before use.

At the time of injection, animals (approximately 6 weeks old) were anesthetized with Isoflurane (3% induction, 1.25% maintenance) and mounted in a stereotaxic frame (Kopf Instruments, USA). Eye ointment was applied and the incision area was infiltrated with durocaine. A longitudinal incision was made along the animal's head and a small craniotomy was performed over the striatum (1 mm rostral and 1 mm lateral to the bregma; (Franklin and Paxinos, 2008)).

Adenoviral vectors (500 nL) were injected through a glass micropipette attached to a syringe via flexible tubing, positioned over the striatum (2.5 mm depth from skull), at a rate of approximately 100 nL/min. After injections, glass micropipettes were left in place for another 5 min to allow the virus to diffuse at the injection site and then were slowly removed. Finally, the

skin was sutured with an absorbable thread, analgesics were subcutaneously administered (Fluxinin 2.5 mg/kg) and animals were kept on a thermostatic blanket until they recovered from anesthesia.

The distribution of ACC-CS neurons across layers was quantified from brain slices obtained from control animals (N = 5) used in preliminary test to set up viral vectors injection parameters. We based our analysis on the caudal part of the ACC (from 1.3 to 0.5 mm anterior to bregma), as it is the area that more densely projects to the DMS. For that, 5 weeks after viral vectors injections mice were deeply anesthetized, transcardially perfused with Phosphato Buffer Saline 0.1 M (PBS) followed by 4% paraformaldehyde in PBS. Brains were dissected out, kept overnight in the same fixative at 4 °C, and stored in 0.1 M PB containing 15% sucrose at 4 °C for 24–72 h. Coronal brain sections were serially cut with a microtome with a freezing stage (40 um) and stored free floating in PBS containing 0.1% sodium azide at 4 °C until use. Images of labeled neurons were acquired with an epifluorescence microscope (Axio Imager.M2, Zeiss) equipped with structured light illumination (Apotome.2, Zeiss) with a 20x objective. Labeled neurons were detected using a custom-made scripts based on the Matlab Image Processing Toolbox as previously described (Kasanetz and Nevian, 2021). Briefly, images were low-pass filtered (Wiener method) and background (estimated by morphological opening) was subtracted. Then, ROIs were segmented to find circular objects about the size of cell bodies using circular Hough transform (imfindcircles function in Matlab) and objects with mean fluorescence intensities above five times the background standard deviation were considered positive.

### Spared nerve injury of the sciatic nerve

About three weeks after intrastriatal viral vectors injection, mice were anesthetized with Isoflurane (3% induction, 1.25% maintenance), eye ointment was applied and fur was shaved from the left thigh. An incision was made in order to expose the sciatic nerve and the peroneal and tibial nerve branches were ligated using a silk tread. Then an axotomy was performed posterior to the ligation, leaving the sural nerve branch intact. The skin was then sutured with an absorbable thread and animals were kept on a thermostatic blanket until they recovered from anesthesia. The animals were controlled on a regular basis during the following week. Control animals (sham) received the same treatment with the difference that the sciatic nerve was exposed but not injured. The assignment of each mouse to each treatment was done randomly.

### Von Frey test

The mechanical threshold of the hindpaw was evaluated before and after sciatic nerve injury (Fig. 1(**B**)) with the Von Frey test as previously described (Blom et al., 2014; Santello and Nevian, 2015; Santello et al., 2017; Kasanetz and Nevian, 2021). Mice were individually placed on a raised wire mesh inside Plexiglas compartments and allowed to habituate for 30 min. The mechanical threshold was then tested using an Electronic Von Frey aesthesiometer (IITC Life Science, CA, USA) by slowly applying pressure to the lateral plantar surface of the hind-paw (area innervated by the sural nerve) with the Von Frey filament until a paw withdrawal was evoked. Six pressure measures were taken per each hind-paw and an unpaired t-test was used as exclusion/inclusion criterion.

### Slice preparation

Electrophysiological recording were performed between 2 and 6 weeks after sciatic nerve lesion. Mice were deeply anesthetized with Isoflurane and decapitated. The brain was quickly removed and sliced (300 um) in the coronal plane using a vibratome (Ted Pella) in a low calcium artificial cerebro-spinal fluid solution (Low-Ca ACSF) at 4 °C (in mM: 125 NaCl, 2.5KCl, 1.25 Na2HPO4, 10 glucose, 25 NaHCO3, 2 MgCl2, 1 CaCl2, pH 7.3–7.4 when bubbled with 95% O2/ 5% CO2). Brain slices containing the ACC were stored for 40 min at 28–30 °C in a Low-Ca ACSF equilibrated with 95% O2-5% CO2 and then kept in the same solution at room temperature until recording, as described previously (Kasanetz and Manzoni, 2009; Kasanetz et al., 2013). For recording, slices were placed in a submersion chamber under a Leica DLMS microscope equipped with IR-DIC optics and superfused at 2 ml/min with oxygenated ACSF (similar as Low-Ca ACSF but with 1 MgCl2 and 2 CaCl2) at 28–30 °C.

### Electrophysiology

Whole cell patch-clamp recordings were obtained from cortico-striatal ACC neurons located in deep layers of caudal ACC identified under fluorescence illumination using a Nikon lamp. Cells from superficial layer 5 were preferentially targeted. For each neuron, the approximate location on the anteroposterior axis of the slice in which it was recorded was established using the corpus callosum as a landmark. Pipettes pulled from borosilicate glass (4–7 MΩ), were filled with an intracellular solution suited for current clamp recording (in mM): 130 potassium gluconate, 5 KCl, 10 HEPES, 0.2 EGTA, 2 MgCl, 3 NaATP, 0.3 NaGTP, 10 sodium phosphocreatine; pH 7.2–7.4 using KOH.

Recordings were performed with a HEKA EPC 8 amplifier, signals were low-pass filtered at 4 kHz and digitized at 10 kHz using a DigiData 1322 acquisition interface and Clampex acquisition software (Molecular Devices). Signals were analyzed with ClampFit 11 (Molecular Devices).

Hyperpolarizing current steps (50–400 pA; 500 ms) applied at the soma were used to calculate resting input resistance (Ri) and SAG ratio. Ri was estimated from Ohm's law while SAG ratio = dVm max / dVm ss, where dVm max is the maximal hiperpolarization (substracted Vm at rest) and dVm ss is the voltage reached a few milliseconds before the end of the step (substracted Vm at rest) (Fig. 2(**C**)). Intrinsic excitability was studied by quantifying the firing of action potentials

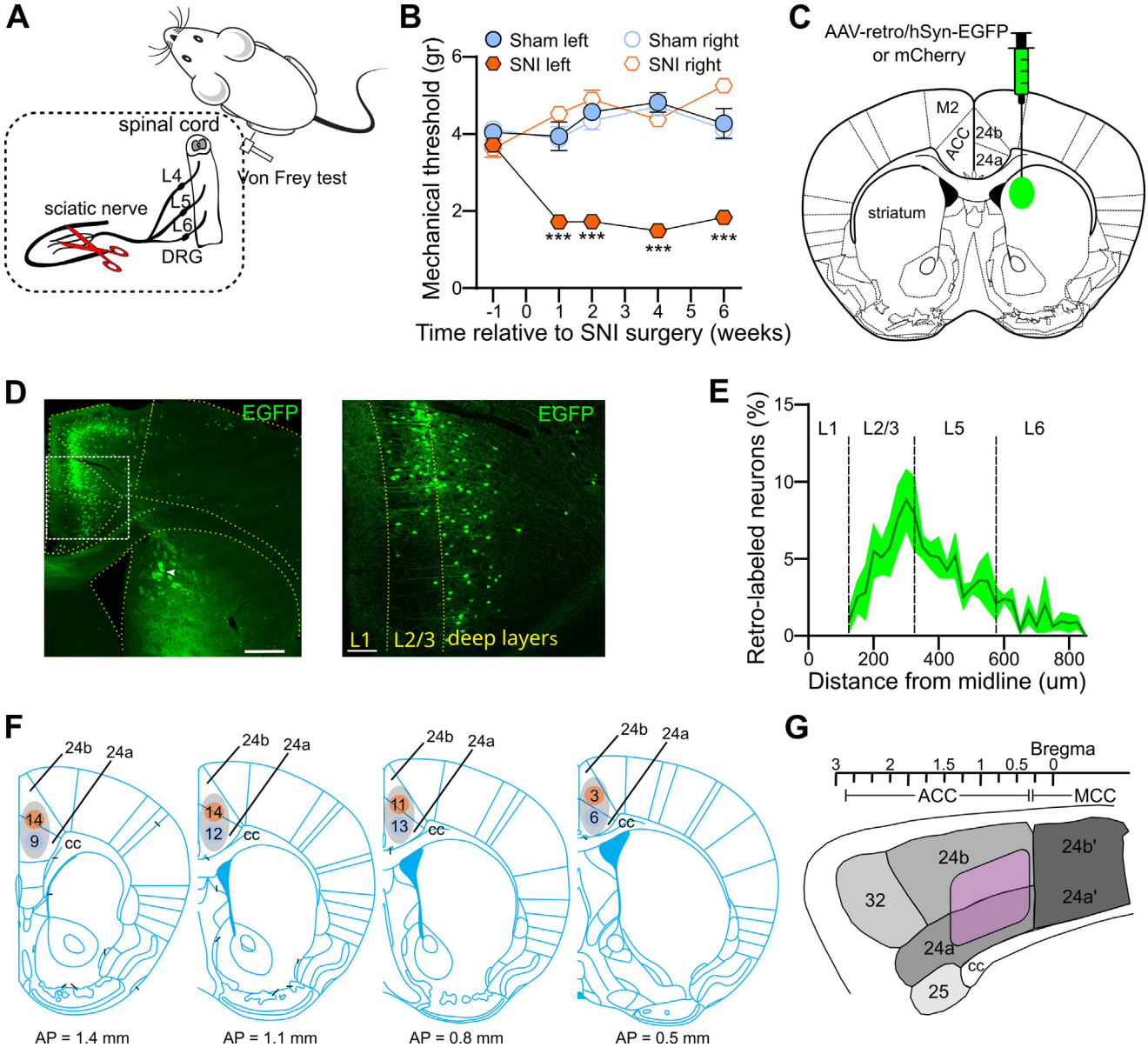


**Fig. 1.** Methodology to assess plastic changes in ACC-CS neurons during experimental neuropathic pain. (**A**) Schematic representation of the SNI model of NP in mice induced by cutting two of the three branches of the sciatic nerve. The lesion-induced allodynia was estimated from the mechanical threshold necessary to evoke paw withdrawal using an electronic Von Frey aesthesiometer. (**B**) Compared to sham, SNI mice showed a reduction in the mechanical threshold of the injured, but not in the intact, hindpaw (SNI $n = 15$; sham $n = 14$; $^{***}P < 0.001$, 3-way ANOVA). Mean ± SEM is depicted. (**C**) Schematic representation of the injection in the DMS of a viral vector for retrograde infection used to label ACC-CS neurons. (**D**) Microphotographs showing the fluorescence spot at the injection site and labeled neurons in the ACC (left, scale bar = 500 um). Further magnification of the image centered in the ACC (right, scale bar = 100 um). (**E**) Frequency distribution of labeled neurons respect to their distance from midline. Line and shaded areas represent mean and sem, respectably; $n = 5$. (**F**) Schematic drawings of coronal sections of the mouse brain illustrating the location of neurons recorded along the anteroposterior (AP) axis of the ACC. The number of neurons recorded at each location is indicated for sham (light blue) and SNI (orange) mice. The distance to the bregma of each section is marked. (**G**) Schematic drawings of a sagital section of a mouse brain depicting the different subregions of the ACC according to Vogt and Paxinos (Vogt and Paxinos, 2014). The purple area represents the region covered by our recordings, located in the caudal half of the ACC.

in response to a series of 500 ms depolarizing current steps. The rheobase was calculated as the intensity of the smallest current step capable of inducing an action potential. To better quantify the input/output relationship (tuning curve), current vs firing curves were aligned to the first current step inducing firing (Fig. 3(**D**)). Then, each curve was fitted with a one-phase association exponential equation (Fig. 3(**E**)) as follows: Y = Y0 + (Plateau-Y0)*(1-exp(-K*x)), where the plateau is the cell maximal firing attainable and K is the rate constant. Two neurons per group were discarded after this analysis since the fit was not statistically significant.

Synaptic transmission was evaluated by recording EPSP evoked by electric stimulation (0.2 ms pulse duration) of distal afferents with a glass pipette (typically in layer 1 or on the border between layer 1 and 2). It is

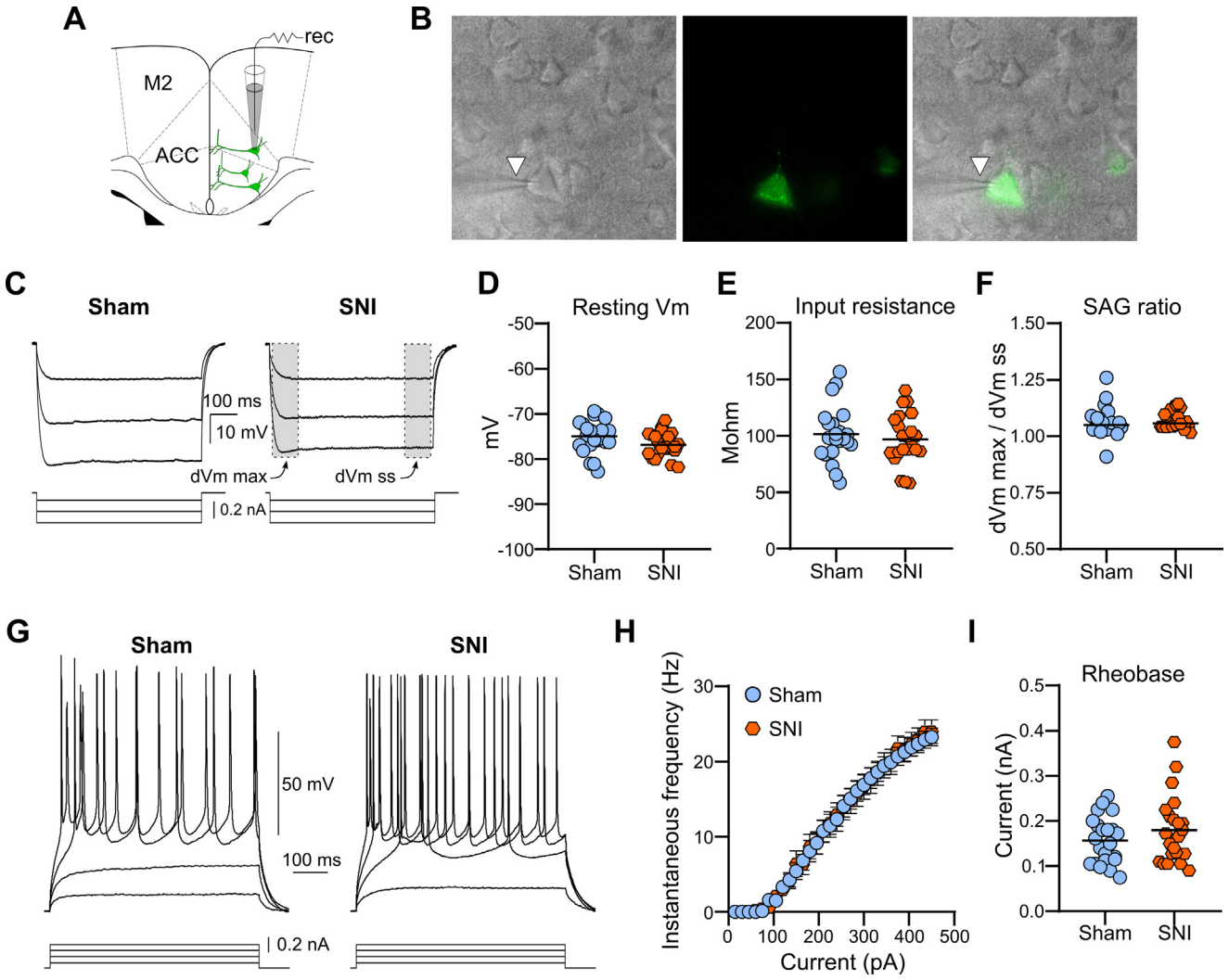


**Fig. 2. ACC-CS neurons from SNI and sham mice exhibited similar intrinsic excitability.** (**A**) Representation of the configuration used to record ACC-CS neurons in brain slices of mice. (**B**) Microphotograph showing the identification of ACC-CS neurons during patch clamp recording based on its fluorescence. Images under infrared (left) or fluorescent (center) illumination are depicted. Right: composed image. Arrowhead marks the recording electrode. (**C**) Representative traces showing voltage membrane responses to a series of negative current steps. (**D**) Resting membrane potential and input resistance were similar between SNI and sham (SNI $n = 22$; sham $n = 22$). (**E**) SAG ratio were small ( < 20%) for most of the cells recorded in both groups. (**F**) Representative traces of membrane depolarization in response to positive somatic current steps. (**G**) Firing frequencies and rheobase were similar between groups (SNI $n = 22$; sham $n = 22$). Population data is represented with Mean ± SEM (**H**); Horizontal lines are mean (**D**, **E**) or median (**F**, **I**) values. dVmax = maximal hiperpolarization; dVm ss = steady state hyperpolarization.

important to bear in mind that this type of stimulation give rise to high between-neurons variability in EPSP amplitudes, since it will depend in part on the number of stimulated axons, which varies from slice to slice depending on the positioning (blind in relation to the axons) of the electrode. However, the consistency in the location of the electrode and a high number of tested cells normally allow to uncover group differences, if they exist. Single pulses or trains of two or five pulses at 50 Hz with increasing stimulation intensities were employed. Each configuration of train-intensity was applied at least eight times every 10 s and the average trace was obtained for further analysis. Stimulation trials that triggered action potentials were not considered for EPSP measurements. EPSP amplitude is the difference between the peak Vm in the response window and a baseline value measured just before stimulation. After train stimuli, baseline values were calculated before each stimulus of the train. Maximal train depolarization corresponds to the peak Vm in the response window, considering all EPSPs (Fig. 4(**A,G**)). Normalized depolarization amplitudes were obtained by dividing the Vm attained during each EPSP to the amplitude of the first EPSP of the train. EPSP decay times were estimated as the area / amplitude, assuming that EPSP kinetics can be adjusted to a sum of exponentials. Half-width of EPSP was the EPSP duration at the half amplitude membrane depolarization. Synaptically-driven firing was quantified during trains of five pulses, as single or double stimuli rarely induced firing.

Paired-pulse ratio of EPSC were recording in voltage clamp mode with a holding potential of −70 mV in the presence of the GABA-A receptor blocker Picrotoxin (50 uM). Access resistance was evaluated with 2-mV

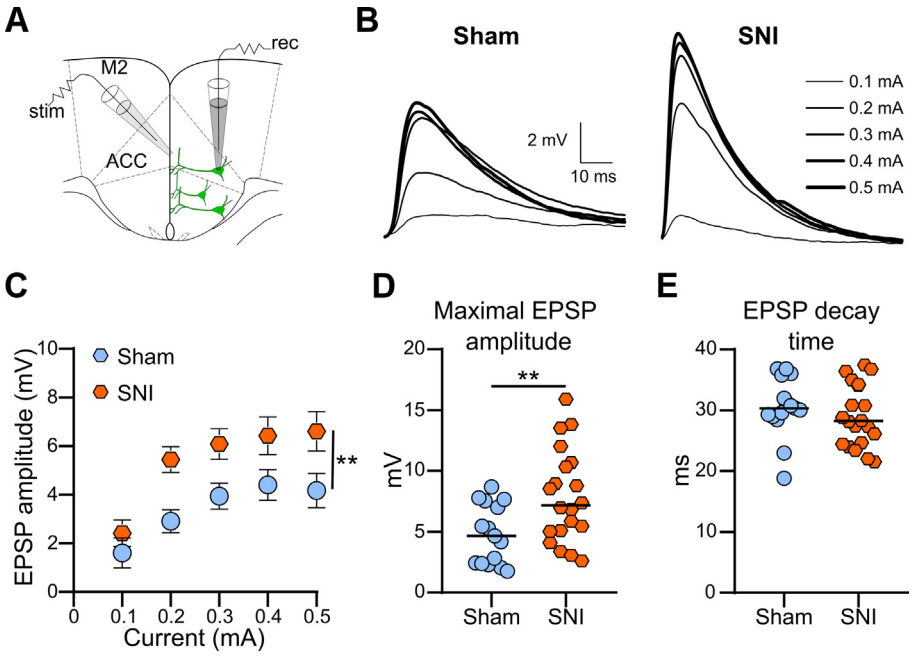


**Fig. 3. Increased EPSP in response to layer 1 stimulation in ACC-CS neurons from sciatic nerve injured mice.** (**A**) Schematic representation of the configuration used to record EPSP in ACC-CS neurons in response to electrical stimulation of layer 1. (**B**) Representative traces of EPSP obtained in response to increasing stimulation intensities. (**C**) EPSP amplitude as a function of stimulation intensity (**$P$ < 0.01 group effect, Mixed-effects model analysis). (**D**) Maximal EPSP amplitude observed during the stimulation curve (**$P$ < 0.01 t-test). (**E**) EPSP decay kinetics did not differ between groups. For (**C-E**) SNI $n$ = 20, sham $n$ = 15. Population data is represented with Mean ± SEM (**C**); Horizontal lines are mean (**D, E**) values.

hyperpolarizing pulse applied before each EPSC. Cells were rejected if acces resistance was higher than 25 Mohm or changed more than 20% during the experiment.

### Statistical analysis

Statistical analysis was performed with GraphPad Prism 8 (GraphPad Sofware, La Jolla, CA, USA) using a critical probability of $P$ < 0.05. Since for some electrophysiological measurements the variability between cells of the same animal was smaller than the variability between animals, we used animals as experimental units. The values obtained in neurons of the same mouse were averaged. Therefore, throughout the study, N corresponds to the number of mice per group. Data distribution was assessed for normality using D'Agostino & Pearson test. On some occasions, outliers were discarded because they affected the assumption of the statistical analysis. In no case did this change the results of the analyses. A three-way ANOVA (time-lesion-hindpaw) followed by Holm-Sidak's multiple comparisons test was performed to compare for the mechanical threshold before and after sciatic nerve surgery. Statistical significance between groups for individual variables was tested using t-test or the nonparametric Mann Whitney test or Wilcoxon matched-pairs signed rank test. Repeated measures two-way ANOVA or a Mixed-effects model (REML) followed by Holm-Sidak's multiple comparisons test were used to assess differences in X-Y curves. In plots showing individual values, horizontal lines correspond to group mean or median values, depending whether data followed a Gaussian distribution or not.

## RESULTS

### Recording ACC-CS neurons in experimental NP

We used the Spared Nerve Injury (SNI) model of sciatic nerve lesion (Fig. 1(**A**)) to study how NP affects intrinsic and synaptic properties of cACC-CS neurons. Using the electronic Von Frey test we observed that SNI animals developed a mechanical allodynia of the injured hindpaw (left) that lasted for the entire curse of the experiments (maximum six weeks after surgery) (Fig. 1(**B**)). Three-way ANOVA of lesion, time, and hindpaw (left or right), showed a significant difference for the interaction lesion X time X hindpaw ($F(4, 84)$ 66.7, $P$ < 0.001). Post-hoc analysis (Tukey's multiple comparisons test) showed a significant decreased in the mechanical threshold of the injured hind-limb of SNI mice compared to Sham at every session tested after sciatic nerve injury ($P$ < 0.001), but not before ($P$ > 0.05). In contrast, the mechanical sensitivity of the uninjured paw did not differ between groups ($P$ > 0.05).

In order to evaluate intrinsic and synaptic properties of cACC-CS neurons, we performed whole-cell patch clamp recording in brain slices from sham and SNI mice. ACC-CS cells were recognized from the presence of a fluorescent tag encoded by viral vectors of retrograde expression (AAV-retro/2-hSyn1-EGFP or mCherry), previously injected into the DMS (ipsilateral to recorded ACC, contralateral to injured hindpaw, see methods; Fig. 1(**C-D**), 2(**A-B**)). Most of the labeled neurons were found in the caudal part of the ACC (1.3–0.5 mm anterior to bregma), in agreement with the notion that this region give rise to the densest cortical projections to the DMS (Kasanetz et al., 2008; Guo et al., 2015; Hintiryan et al., 2016). Labeled neurons were also observed in more rostral ACC and/or motor cortical regions, probably due to diffusion of viral vectors to ventral or dorso-lateral areas of the striatum, respectably. ACC-CS neurons were distributed between layers 2/3 and 5, with a denser presence in the interface between layer 3 and the superficial parts of layer 5 (Fig. 1(**D-E**)). Thus, to investigate neuronal plasticity in neurons projecting to the DMS, in this study we restricted the recording to ACC-CS neurons located in deep layers of the caudal part of the ACC. A summary of the location of the neurons

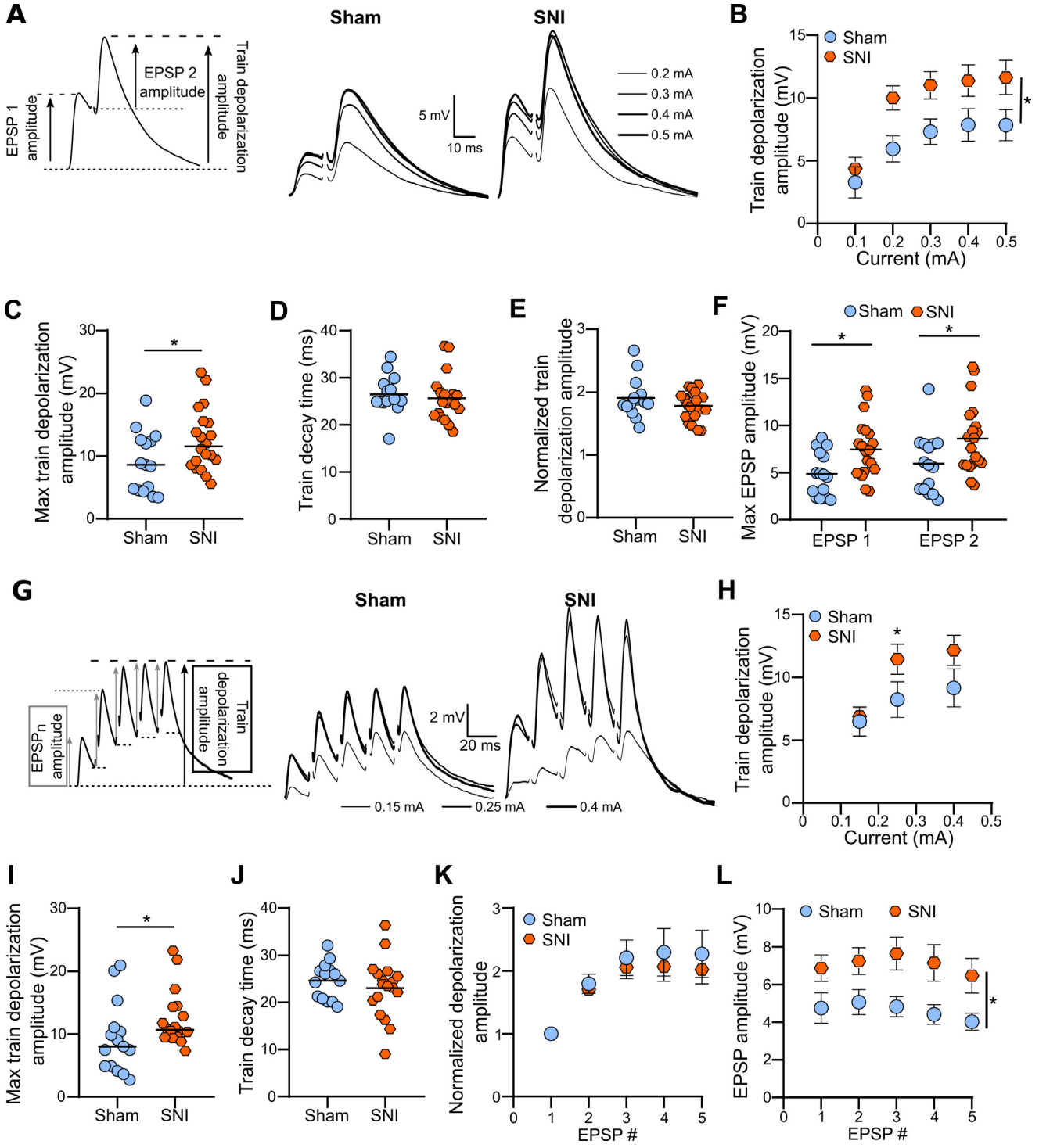


**Fig. 4. Enhanced depolarization with unchanged temporal summation in responses to trains of stimuli in ACC-CS neurons from SNI mice.** (**A**) Left: schematic representation of the parameters used to analyze paired-stimuli induced EPSPs. Right: representative traces of voltage synaptic response to increasing stimulation intensities. (**B**) Paired-stimuli-induced depolarization as a function of stimulation intensity (*$P < 0.05$ group effect, Mixed-effects model analysis). (**C**) Maximal depolarization attained in response to the stimulation curve (*$P = 0.03$ t-test). (**D**) Train decay kinetics did not differ between groups. (**E**) Train depolarization normalized to the amplitude of EPSP 1. (**F**) Maximal EPSP 1 and EPSP 2 amplitudes reached during the stimulation curve (*$P < 0.05$ group effect, Two-way RM Anova). (**G**) Left: schematic representation of the parameters used to analyze the EPSPs triggered by trains of 5 stimuli. Right: representative traces of voltage synaptic response to increasing stimulation intensities. (**H**) Depolarization induced by trains of stimuli as a function of stimulation intensity (*$P < 0.05$ post hoc after Mixed-effects model analysis). (**I**) Maximal depolarization attained in response to the stimulation curve (*$P < 0.05$ Mann Whitney test). (**J**) Train decay kinetics did not differ between groups. (**K**) Depolarization attained after each stimulus of the train normalized to the amplitude of EPSP 1. (**L**) Maximal amplitude of each EPSP that comprise the response to trains of stimuli (*$P < 0.05$ group effect, Two-way RM Anova). For (**B-F**) SNI $n = 20$, sham $n = 15$.For (**H-L**) SNI $n = 18$, sham $n = 15$. Population data is represented with Mean ± SEM (**B, H, K, L**); Horizontal lines are mean (**C, D, E, F, J**) or median (**I**) values.

recorded along the anteroposterior axis of the ACC is shown in Fig. 1(**F-G**). We recorded 40 neurons in 22 sham mice and 42 neurons in 22 SNI mice (1–3 cells per animal).

### Intrinsic excitability of cACC-CS neurons was conserved during NP

In previous studies it was observed that sciatic nerve injury produced an increase in the intrinsic excitability of the pyramidal neurons of layer 5 of the cACC (Blom et al., 2014). This was reflected in a higher input resistance and an augmented firing rate in response to depolarizing currents. In order to assess whether such changes also occur in cACC-CS neurons, we recorded neurons located in layer 5 and evaluated voltage responses to positive and negative current steps applied in the cell body (Fig. 2(**C,F**)). The resting membrane potential (Fig. 2(**D**); t-test: t = 1.895, df = 42, $P$ = 0.07) and the magnitude of the steady state polarization attained during negative current steps (Suppl. Fig. 1A; Two way RM Anova, group effect: F(1,42) = 0.29, $P$ = 0.58; current × group effect: F(7,294) = 0.48, $P$ = 0.84) were similar between cACC-CS neurons from sham and SNI mice. Accordingly, the input resistance did not change in SNI animals (Fig. 2(**E**); t-test: t = 0.641, df = 42, $P$ = 0.52). We also measured the SAG ratio, defined as the ratio between the fast polarization and the steady state induced by hyperpolarizing current steps (Fig. 2 (**C**)). A large SAG ratio (typically > 20%; (Santello and Nevian, 2015)) reflects the presence of H-type currents, characteristic of pyramidal tract (PT), but absent in intratelencephalic (IT) pyramidal neurons (Reiner, 2010; Shepherd, 2013; Meda et al., 2019). We found that SAG ratio was similar between cACC-CS neurons from sham and SNI mice (Fig. 2(**F**); Mann Whitney test, U = 194, $P$ = 0.26), and that only 3 out of 82 recorded cells presented a SAG ratio > 1.2. Therefore, this study was biased towards IT cACC-CS neurons, probably due to their preferential location in superficial layer 5 (Reiner, 2010; Meda et al., 2019), where we observed most of the retrograde labeled neurons.

Then we analyzed action potential firing in response to increasing depolarizing currents steps (Fig. 2(**G**)) and observed comparable firing frequencies between cACC-CS cells from sham and SNI mice (Fig. 2(**H**); Mixed-effects model, group effect: F(1,41) = 0.012, $P$ = 0.91; current × group effect: F(29,1183) = 0.226, $P$ = 0.99). Furthermore, rheobase, the minimum current step capable of inducing action potentials (Fig. 2(**I**); Mann Whitney test, U = 205, $P$ = 0.39) and action potential voltage threshold (Suppl. Fig. 1B; t-test: t = 0.039, df = 40, $P$ = 0.96) were similar between groups. Although these data suggest that NP did not affect the excitability of cACC-CS neurons, the high variability observed in rheobase may have masked more subtle changes in the tuning curves, such as the rate constant and potential maximum firing. To better characterize this, tuning curves were aligned to the first current step inducing firing and fitted with a one-phase association exponential equation (Suppl. Fig. 1C, left). This way we confirmed that the rate constant (t-test: t = 0.1758, df = 41, $P$ = 0.86) and plateau (t-test: t = 1.239, df = 41, $P$ = 0.22) of the tuning curves were undistinguished between cACC-CS neurons from both groups (Suppl. Fig. 1C).

Altogether, this data demonstrated that a SNI of the sciatic nerve did not affect the intrinsic excitability of cACC-CS neurons.

### Increased excitatory post-synaptic potentials in cACC-CS from SNI mice

In order to study if NP modified the strength of synaptic transmission onto cACC-CS neurons, we recorded post-synaptic potentials in response to electrical stimulation of layer 1 (to favor distal afferences; Fig. 3(**A-B**)). We tested excitatory post-synaptic potentials (EPSP) amplitude as a function of stimulation intensity and found larger EPSP in cells from SNI mice (Fig. 3(**C**); Mixed-effects model, group effect: F(1,33) = 7.84, $P$ = 0.008; stim intensity × group effect: F(4,118) = 1.371, $P$ = 0.25). Furthermore, the maximal depolarization attained in response to the stimulation curve was higher in cACC-CS neurons from SNI compared to sham animals (Fig. 3(**D**); t-test: t = 2.754, df = 33, $P$ = 0.009). The increase in EPSP amplitude occurred without changes in its decay kinetics (Fig. 3 (**E**); t-test: t = 0.844, df = 33, $P$ = 0.4).

### cACC-CS neurons from SNI mice presented higher depolarization with conserved temporal summation in response to trains of synaptic inputs

The increase in the magnitude of EPSP may be due to changes in synaptic transmission or altered dendritic integration of synaptic potentials. In fact, both phenomena were observed in cACC neurons during pathological pain (Koga et al., 2015; Santello and Nevian, 2015). We therefore decided to assess whether SNI affected synaptic integration in cACC-CS neurons by analyzing the temporal summation of EPSP evoked by paired stimuli (2-stim, Fig. 4(**A**)) or trains of 5 stimuli (5-stim, Fig. 4(**G**)) at 50 Hz. First, we observed that the depolarization attained during 2-stim protocol was higher in cACC-CS neurons from SNI mice compared to sham (Fig. 4(**B**), Mixed-effects model, group effect: F(1,33) = 4.64, $P$ = 0.03; stim intensity × group effect: F(4,114) = 1.357, $P$ = 0.25; Fig. 4(**C**), t-test: t = 2.15, df = 33, $P$ = 0.03). A similar finding was observed when the 5-stim train was applied (Fig. 5(**H**), Mixed-effects model, group effect: F(1,31) = 2.64, $P$ = 0.11; stim intensity × group effect: F(2,57) = 3.17, $P$ = 0.04, post hoc *$P$ = 0.05; Fig. 5(**I**), Mann Whitney test, U = 75, $P$ = 0.03). Interestingly, in both cases the enlarged responses occurred without changes in synaptic potentials decay time (2-stim: Fig. 4(**D**), t-test: t = 0.524, df = 33, $P$ = 0.60; 5-stim: Fig. 4(**J**), t-test: t = 0.842, df = 30, $P$ = 0.41), suggesting that post-synaptic integration was not affected. In support of this, when the depolarization reached after each stimulus was normalized by the amplitude of the first EPSP, differences between sham and SNI mice were no longer evident (2-stim: Fig. 4(**E**), t-test: t = 1.303, df = 31, $P$ = 0.2; 5-stim: Fig. 4(**K**),

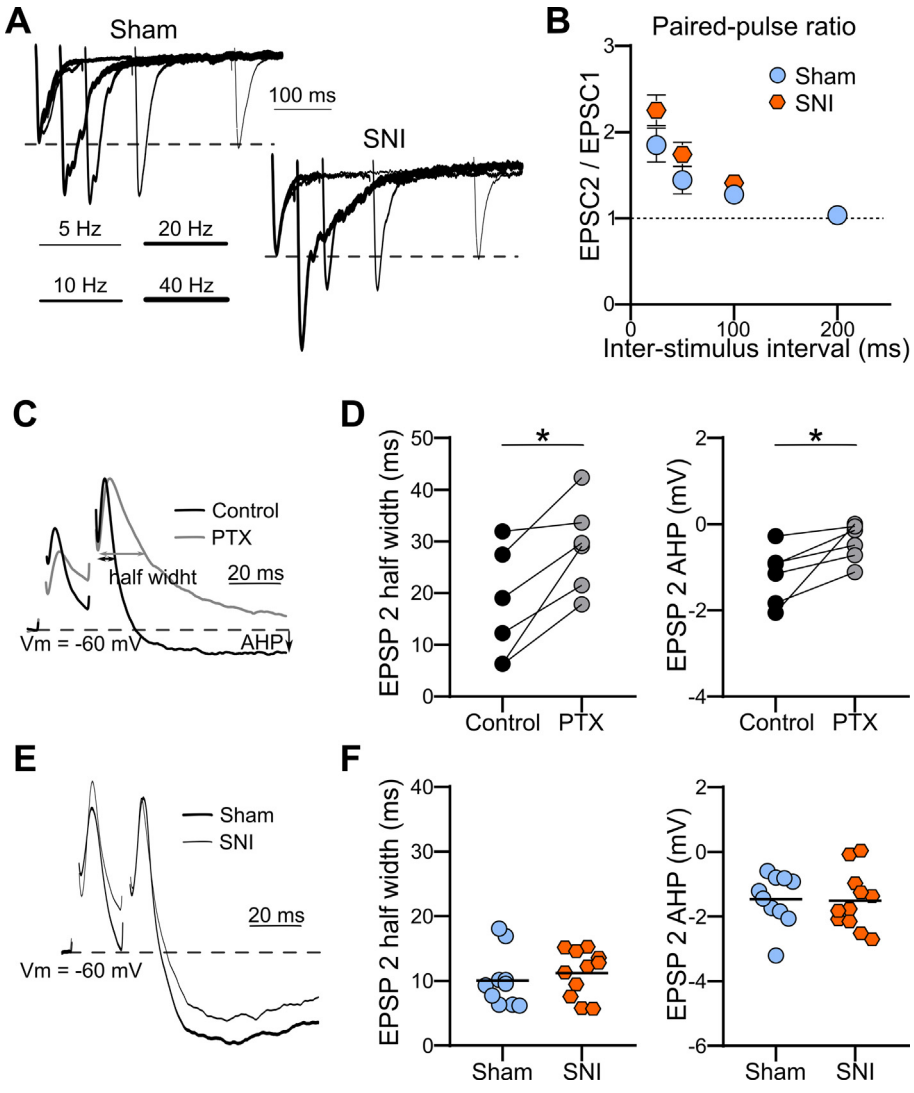


**Fig. 5. Short-term plasticity of evoked EPSC and inhibitory component of synaptic potentials of ACC-CS neurons remained unaltered after sciatic nerve injury**. (**A**) Representative traces of paired-stimulus induced EPSCs in SNI and Sham mice. EPSCs were normalized to the amplitude of the first response. (**B**) Paired-pulse ratio as a function of inter-stimulus interval were comparable between groups. SNI $n = 7$, Sham $n = 7$. (**C**) Representative traces showing the effect of picrotoxine 50 uM (PTX) on the half-width and afterhiperpolarization (AHP) of synaptic potentials induced with an initial membrane potential (Vm) of −60 mV. (**D**) The half-width and AHP were dramatically reduced by PTX (*$P = 0.03$, Wilcoxon matched-pairs signed rank test). (**E**) Representative traces of synaptic potentials induced with an initial Vm of −60 mV in ACC-CS neurons from SNI and Sham animals. (**F**) The half-width and AHP were similar between injured and control mice. In (**C**) and (**E**), the traces were normalized to the EPSP 2 amplitude to better visualize the differences in half-width. Population data is represented with Mean ± SEM (**B**); Horizontal lines are mean (**F**). For (**F**) SNI $n = 11$, sham $n = 10$.

Mixed-effects model, group effect: F(1,31) = 0.291, $P = 0.59$; EPSP # x group effect: F(4,122) = 0.352, $P = 0.84$).

The synaptic integration evaluated here may have been influenced by short-term presynaptic plasticity, which eventually could have hidden putative differences in dendritic integration. To determine if this is the case, we recorded excitatory post-synaptic currents (EPSC) in cACC-CS neurons in response to layer 1 electric stimulation and evaluated presynaptic plasticity by means of the ratio between pairs of EPSC induced with different inter-stimulus intervals (Fig. 5(**A**)). We found that paired-pulse ratio curves were similar between sham and SNI mice (Fig. 5(**B**); Two-way RM ANOVA, group effect: F(1,12) = 2.35, $P = 0.15$; inter-stimulus interval × group effect: F(4,48) = 1.28, $P = 0.29$).

Altogether the data indicates that synaptic potentials onto cACC-CS neurons were larger after SNI as a result of a strengthened synaptic transmission. This conclusion is supported by the fact that the amplitude of each of the EPSP that make up the responses to trains of stimuli (see scheme in Fig. 4(**A,G**)) were higher in SNI compared to sham mice (2-stim: Fig. 4(**F**), Two-way RM ANOVA, group effect: F(1,33) = 6.79, $P = 0.01$; EPSP # x group effect: F(1,33) = 0.006, $P = 0.93$; 5-stim: Fig. 4(**L**), Two-way RM ANOVA, group effect: F(1,31) = 6.23, $P = 0.05$; EPSP # x group effect: F(4,124) = 0.382, $P = 0.82$).

We recorded EPSPs in the absence of GABA-A channel blockers, in order to obtain a physiological readout of layer 1 stimulation. Therefore, we cannot rule out that the recurrent activation of inhibitory interneurons may have influenced the results obtained. This is unlikely, since inhibitory post-synaptic potentials (IPSP) typically shape the kinetics of EPSP, contrary to what we have observed here, where EPSP were larger in SNI mice without changes in decay time. Furthermore, in a fraction of cells we recorded synaptic potentials in response to paired stimuli while holding the membrane potential at −60 mV to favor the manifestation of inhibitory potentials, which in our recording configuration reversed at −70 mV. Under these conditions, the synaptic potentials exhibited a shorter half-width than that observed at resting membrane potential, and a prominent after-hyperpolarization (AHP) (Fig. 5(**C**)). Upon application of the GABA-A receptor blocker picrotoxin (50 uM), synaptic potentials became longer (Fig. 5(**C-D**); Wilcoxon matched-pairs signed rank test, W = 21, $P = 0.03$), and the AHP was significantly attenuated (Fig. 5(**C-D**); Wilcoxon matched-pairs signed rank test, W = 21, $P = 0.03$), evidencing the role of GABAergic synapses in these phenomena. We found

that the half-width of synaptic potentials (Fig. 5(**E,F**) left; t-test: t = 0.677, df = 19, $P = 0.51$) and the AHP (Fig. 5(**E, F**) right; t-test: t = 0.146, df = 19, $P = 0.88$) were similar between neurons from injured and control animals.

Altogether, our data suggest that changes in excitatory inputs might be the main mechanism at the origin of the larger EPSP recorded in cACC-CS from SNI mice.

### Enlarged EPSP in cACC-CS neurons after sciatic nerve injury were associated with increased synaptically-driven action potential firing

We finally investigated whether the larger EPSPs that were observed in cACC-CS from SNI mice yielded functionally relevant consequences. For that we quantified action potential firing during trains of 5 synaptic stimuli (Fig. 6(**A**)). The proportion of cells firing at least once during the stimulation protocol was slightly higher in SNI mice, specially for intermediate stimulation intensities (Fig. 6(**B**)). Furthermore, cACC-CS neurons from SNI mice fired more synaptically-evoked action potentials during the trains (Fig. 6(**C**), Two-way RM ANOVA, group effect: F(1,31) = 2.67, $P = 0.11$; stim intensity × group effect: F(2,62) = 3.13, $P = 0.05$, post hoc $^*P < 0.05$). Notably, this was not solely the result of more cACC-CS active cells, since when considering only the active neurons, firing was still larger in injured animals (Fig. 6(**D**), Two-way RM ANOVA, group effect: F(1,9) = 2.93, $P = 0.12$; stim intensity × group effect: F(2,18) = 3.72, $P = 0.04$, post hoc $^*P < 0.05$). Since the rheobase (Fig. 2(**I**)) and voltage threshold (Suppl. Fig. 1B) for somatic action potential generation, and the temporal summation of EPSP (Fig. 4(**K**)) were similar in sham and SNI mice, the increased firing was most likely due to synaptic mechanisms.

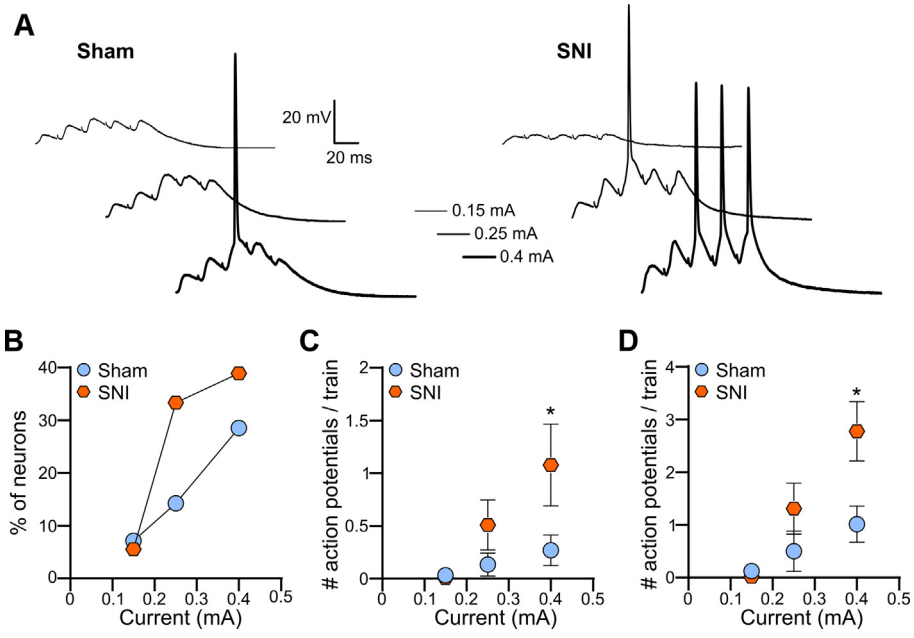


**Fig. 6. Augmented synaptically-evoked action potential firing in ACC-CS neurons from SNI mice.** (**A**) Representative traces of synaptic potentials (AP) induced by trains of 5 stimuli with increasing stimulation intensities. Note in some occasions action potentials coupled to EPSPs. (**B**) Percentage of neurons that fired synaptically-evoked AP as a function of stimulation intensity. (**C-D**) Number of AP induced per train-stimulus as a function of stimulation intensity ($^*P < 0.05$ post hoc after Two way RM Anova). In (**C**) all tested cells were considered; SNI $n = 18$, sham $n = 15$. In (**D**) only cells showing synaptically-evoked firing were considered; SNI $n = 7$, sham $n = 4$. Population data is represented with Mean ± SEM (**C-D**).

## DISCUSSION

One of the main clinical features of chronic pathological pain is the affective, motivational, and cognitive deficits that are co-morbid with the pain. This may be, at least partially, mediated by synaptic and cellular alterations in the meso-cortico-limbic system (Apkarian et al., 2005; Bushnell et al., 2013; Baliki and Apkarian, 2015; Da Silva and Seminowicz, 2019). Neuronal plasticity have been extensively investigated in the ACC, a main cortical substrate of pain affect and descending pain modulatory system, and was found that NP-induced synaptic and dendritic modifications underlie ACC hyperactivity (Zhang et al., 2017; Sellmeijer et al., 2018; Zhou et al., 2018; Kasanetz and Nevian, 2021) and are required for the behavioral manifestation of nociceptive sensitization (Koga et al., 2015; Santello and Nevian, 2015; Santello et al., 2017; Li et al., 2021, 2010). Here we investigated neuronal plasticity in a rodent model of NP and reported for the first time unequivocally that cACC neurons projecting to the DMS are engaged in pathological plasticity. Specifically, distal inputs onto cACC-CS neurons were strengthened in SNI mice resulting in enhanced synaptically-induced firing. These changes may render the cACC-CS pathway more likely to be activated by noxious stimuli and participate in the brain circuits that sustain pathological pain. In agreement with this idea, optogenetic inhibition of cACC-CS pathway reverted mechanical and thermal sensitization associated to NP (Zhuang et al., 2019).

Neuronal plasticity in the cACC associated with pathological pain is not uniform across layers (Li et al., 2010; Blom et al., 2014; Koga et al., 2015; Santello and Nevian, 2015) and may differ also between projection cell types (see below). To correctly integrate our findings into a model of pathological activity of cACC microcircuits, it is crucial to clearly identify the subtype of neurons under study. Our recording were biased towards IT cortico-striatal pyramidal neurons of superficial layer 5, as evidenced by the lack of a prominent SAG ratio in the membrane responses to hyperpolarizing current steps. Thus, plastic changes upon NP in PT cACC-CS neurons may differ from the finding reported here. In this line, a recent study showed subtle differences in the neuronal plasticity expressed by cortico-cortical IT and cortico-

thalamic PT ACC neurons in SNI mice (Meda et al., 2019).

In order to uncover aberrant neuronal plasticity in cACC-CS neurons during NP we first studied intrinsic membrane excitability and found that membrane properties were unchanged in SNI mice, including the firing frequency of action potentials in response to depolarizing current steps. Increased intrinsic excitability was observed in previous studies recording rACC neurons projecting to other subcortical regions (Meda et al., 2019; Gao et al., 2020) or cACC cells non-identified regarding its projection sites (Blom et al., 2014). Thus, this mechanism of enhanced excitability may occur in a subgroup of layer 5 ACC neurons, in which IT cACC-CS neurons would not be included. On the other hand, we found that synaptic potentials induced by electrical stimulation of layer 1 were enhanced in neurons from NP animals. This result was very robust, being observed both in responses to single stimuli and in each of the post-synaptic potentials that compose the responses to trains of stimuli. Furthermore, synaptic inputs were accompanied by an increased rate of action potential firing in a subset of cACC-CS neurons from SNI animals. The absence of a general increase in excitability could mean that these neurons would not be spontaneously hyperactive in vivo during NP, but rather that they would be more likely to be recruited by the activation of specific synaptic pathways under particular circumstances; i.e. neuropathic noxious stimulation. We have recently shown that NP in mice was associated with increased spontaneous activity in deep layers of the cACC without an expansion of the ensemble of neurons activated by strong noxious stimuli (Kasanetz and Nevian, 2021). In these scenario of stable nociceptive representation in the cACC, a facilitated recruitment of cACC-CS neurons would be on expense of other cell types, like PT neurons, which are suppressed by medio-dorsal thalamic inputs to rACC in mice models of NP (Meda et al., 2019). In addition, cACC-CS cells may be more suitable to be activated by weak somatic stimuli, potentially contributing to the allodynic state that characterized pathological pain.

The mechanism underlying the synaptic strengthening of cACC-CS has yet to be fully understood. On the one hand, long-term potentiation-like modifications could explain an increase in synaptic input. Several studies reported in the last decade increases in excitatory synaptic transmission compatible with processes of synaptic plasticity on cACC neurons of layers 2/3 (for review see Bliss et al., 2016) and layer 5 (Chen et al., 2014; Hogrefe et al., 2022). The synaptic enhancement onto layer 5 cACC neurons of NP mice was observed in spinal cord-projecting cells (Chen et al., 2014) or in neurons not identified regarding its projection site (Hogrefe et al., 2022), so it is plausible that cACC-CS studied here underwent a similar process. Alternatively, changes in dendritic integration could have amplify synaptic inputs. However, we observed that the temporal summation of EPSP in cACC-CS was conserved in SNI mice, suggesting that dendritic integration remain intact during NP. In contrast to this, a previous work reported enhanced dendritic summation of EPSP mediated by a decrease in H-type currents in cACC layer 5 neurons during NP (Santello and Nevian, 2015). Although in that work neurons were not identified by their projection site, the study was biased towards neurons with prominent SAG, presumably PT pyramidal cells. Finally, changes in inhibitory transmission could contribute to the increased EPSPs in SNI mice. In fact, a drop in connectivity between layer 5 interneurons and pyramidal cells of the cACC was observed NP animals (Blom et al., 2014). Although a mechanism mediated by interneurons cannot be ruled out, our data suggest that their contribution to the changes found in the EPSP amplitude of SNI mice would be minor. This is based on the fact that EPSP parameters that are highly modulated by recurrent inhibition (i.e. EPSP half width and AHP) were similar between control and NP animals.

The electrical stimulation of layer 1 that we performed here does not allow us to discriminate the origin of these axons. It is possible that our results reflect the combination of several different inputs, and that the observed changes in synaptic potentials are specific to one or various sites of interest for nociceptive information processing, such as the anterior and medial thalamus, amygdala, and the contralateral ACC. Two recent studies addressed input-specific changes in synaptic inputs into ACC neurons during NP. As stated above, Hogrefe et. al (Hogrefe et al., 2022) reported an anterior thalamic nuclei (ATN) to layer 5 cACC neurons-specific enhancement of synaptic transmission in NP mice, while recording cACC neurons not identified regarding its projection site. For their part, Meda et. al. (Meda et al., 2019) observed a decrease excitation/inhibition balance of mediodorsal thalamic input on PT rACC pyramidal neurons. Given this antecedents, it is possible that our data reflect changes in ATN synaptic input, although this needs to be confirmed by future experiments. In any case, changes in connectivity between ATN and ACC-CS could contribute to emotional and cognitive consequences of pathological pain. The ATN is implicated in memory formation and emotional processing and is connected to structures of the limbic system (Nishio et al., 2011; Jankowski et al., 2013). Also, changes in ATN activity were related to nociceptive hypersensitivity (Liu et al., 2017). Further studies are needed to better understand the precise role of ATN to ACC pathway in the experience of pain.

The data presented here were obtained from male mice. Given the known gender differences in acute and chronic pain sensitivity and pain modulation mechanisms, it remains to be determined whether the same effects of NP on cACC-CS neurons occur in female mice.

An increase in the flow of information through IT cACC-CS neurons may have widespread consequences for the brain networks that process and modulate nociception. First and most obvious, it would lead to greater activation of the basal ganglia through the DMS. The striatum is composed of two types of principal neurons that give rise to the direct and indirect pathways of the basal ganglia (Albin et al., 1989), and that play antagonistic roles in motor functions (Kravitz et al., 2010; Kravitz and Kreitzer, 2012) and, presumably, in

the motivational modulation of goal-directed actions (Lobo et al., 2010; Kravitz and Kreitzer, 2012; Kravitz et al., 2012). Thus, the way in which the pathological plasticity of the cACC-CS impacts on each of the two striatal pathways will determine how information flows downstream and its consequences for the experience of pain. In addition, through local collaterals, cACC-CS neurons could contribute to the hyperactivity of other cACC pyramidal neurons, such as those that project to the periaqueductal gray and are involved in descending pain control (Jercog et al., 2021; Lee et al., 2022). Finally, through the typical contra-lateral cortico-cortical projections of IT pyramidal neurons (Reiner, 2010; Shepherd, 2013), responses to nociceptive stimuli would be more likely to spill over to the contra-lateral cACC, resulting in abnormal inter-hemispheric synchronization (Shepherd, 2013). This could be further accentuated if the changes reported here in cACC-CS were extended to the cACC ipsilateral to the injured limb. Interestingly, abnormal inter-hemispheric synchronization has been observed in neurological conditions, including pathological pain (Shepherd, 2013; Qi et al., 2016; Zhang et al., 2022).

Accumulating evidence suggests that the pathophysiology of pain is not uniform in the different domains of the corticostriatal pathway. On the one hand, our results suggest that the cACC-DMS connection would be hyperactive during NP, while its inhibition reverses the noxious sensitization (Zhuang et al., 2019). On the other hand, although a similar scenario was described for rACC-CS neurons (Gao et al., 2020), another study demonstrated rACC hypoactivity associated with inflammatory pain-related anxiety expression (Ducret et al., 2022). Since some of these cells might be corticostriatal, this suggests that hyperactivity and hypoactivity concomitantly spread to the basal ganglia during chronic pain, probably in a time- and pain-type-dependent manner. In this sense, it has been shown that neurons of the prelimbic cortex, a region adjacent to the rACC are hypoactive in NP in rodents, and that the activation of the prelimbic cortico-striatal pathway relieved sensory and affective symptoms (Lee et al., 2015). The way different frontal cortical inputs are integrated by striatal neurons may shed light on the functional organization of cortico-limbic channels during pathological pain (Ren et al., 2021).

In conclusion, the experiments presented here demonstrate that experimental NP engage cACC-CS neurons projecting to the DMS in abnormal neuronal plasticity. Larger synaptic responses associated with increased action potential firing render this pathway more excitable to spread out nociception-related activity through the basal ganglia. This may have consequences for the processing of motivational and cognitive connotations of pathological pain.

## ADDITIONAL INFORMATION

The author(s) declare no additional interests related to this study. The original datasets generated for this study are available from the corresponding author upon reasonable request.

## AUTHOR CONTRIBUTIONS

F.K. designed research; M.J.T., C.I. and F.K. performed research; M.J.T. and F.K. analyzed data; M.J.T., C.I. and F.K. edited the paper; F.K. wrote the paper.

## ACKNOWLEDGEMENTS

We thank Jésica Unger, Verónica Risso, Graciela Ortega, Bárbara Giugovaz and Germán La Iacona for technical assistance. This work was supported by FONCYT – Agencia I + D + I (PICT 2018-0835, 2018-0003), CONICET (PIP 2020-0923) and Ministerio de Ciencia, Tecnología e Innovación-CONICET (Bilateral Cooperation Programme – Call 2016), Argentina; and IBRO (Return Home Fellowship).

## REFERENCES

Albin RL, Young AB, Penney JB (1989) The functional anatomy of basal ganglia disorders. Trends Neurosci 12:366–375. https://doi.org/10.1016/0166-2236(89)90074-X.

Apkarian AV, Bushnell MC, Treede R-D, Zubieta J-K (2005) Human brain mechanisms of pain perception and regulation in health and disease. Eur J Pain 9:463. https://doi.org/10.1016/j.ejpain.2004.11.001.

Baliki MN, Apkarian AV (2015) Nociception, pain, negative moods, and behavior selection. Neuron 87:474–491. https://doi.org/10.1016/j.neuron.2015.06.005.

Baliki MN, Petre B, Torbey S, Herrmann KM, Huang L, Schnitzer TJ, Fields HL, Apkarian AV (2012) Corticostriatal functional connectivity predicts transition to chronic back pain. Nat Neurosci 15:1117–1119. https://doi.org/10.1038/nn.3153.

Ballantine HT, Cassidy WL, Flanagan NB, Marino R (1967) Stereotaxic anterior cingulotomy for neuropsychiatric illness and intractable pain. J Neurosurg 26:488–495. https://doi.org/10.3171/jns.1967.26.5.0488.

Berthier M, Starkstein S, Leiguarda R (1988) Asymbolia for pain: a sensory-limbic disconnection syndrome. Ann Neurol 24:41–49. https://doi.org/10.1002/ana.410240109.

Bliss TVP, Collingridge GL, Kaang B-K, Zhuo M (2016) Synaptic plasticity in the anterior cingulate cortex in acute and chronic pain. Nat Rev Neurosci 17:485–496. https://doi.org/10.1038/nrn.2016.68.

Blom SM, Pfister J-P, Santello M, Senn W, Nevian T (2014) Nerve injury-induced neuropathic pain causes disinhibition of the anterior cingulate cortex. J Neurosci 34:5754–5764. https://doi.org/10.1523/JNEUROSCI.3667-13.2014.

Breivik H, Collett B, Ventafridda V, Cohen R, Gallacher D (2006) Survey of chronic pain in Europe: prevalence, impact on daily life, and treatment. Eur J Pain 10:287. https://doi.org/10.1016/j.ejpain.2005.06.009.

Büchel C, Bornhövd K, Quante M, Glauche V, Bromm B, Weiller C (2002) Dissociable neural responses related to pain intensity, stimulus intensity, and stimulus awareness within the anterior cingulate cortex: a parametric single-trial laser functional magnetic resonance imaging study. J Neurosci 22:970–976. https://doi.org/10.1523/JNEUROSCI.22-03-00970.2002.

Bushnell MC, Čeko M, Low LA (2013) Cognitive and emotional control of pain and its disruption in chronic pain. Nat Rev Neurosci 14:502–511. https://doi.org/10.1038/nrn3516.

Chen T, Koga K, Descalzi G, Qiu S, Wang J, Zhang L-S, Zhang Z-J, He X-B, Qin X, Xu F-Q, Hu J, Wei F, Huganir RL, Li Y-Q, Zhuo M (2014) Postsynaptic Potentiation of Corticospinal Projecting Neurons in the Anterior Cingulate Cortex after Nerve Injury 1744-8069-10–33. Mol Pain 10. https://doi.org/10.1186/1744-8069-10-33.

Cordeiro Matos S, Zhang Z, Seguela P (2015) Peripheral Neuropathy Induces HCN Channel Dysfunction in Pyramidal Neurons of the

Medial Prefrontal Cortex. J Neurosci 35:13244–13256. https://doi.org/10.1523/JNEUROSCI.0799-15.2015.
Costigan M, Scholz J, Woolf CJ (2009) Neuropathic pain: a maladaptive response of the nervous system to damage. Annu Rev Neurosci 32:1–32.
Da Silva JT, Seminowicz DA (2019) Neuroimaging of pain in animal models: a review of recent literature. Pain Rep 4:e732.
Derbyshire SWG, Jones AKP, Creed F, Starz T, Meltzer CC, Townsend DW, Peterson AM, Firestone L (2002) Cerebral responses to noxious thermal stimulation in chronic low back pain patients and normal controls. Neuroimage 16:158–168. https://doi.org/10.1006/nimg.2002.1066.
Ducret E, Jacquot F, Descheemaeker A, Dallel R, Artola A (2022) Chronic facial inflammatory pain-induced anxiety is associated with bilateral deactivation of the rostral anterior cingulate cortex. Brain Res Bull 184:88–98. https://doi.org/10.1016/j.brainresbull.2022.03.012.
Franklin KBJ, Paxinos G (2008) The mouse brain in stereotaxic coordinates, Compact. 3rd ed. Amsterdam Heidelberg: Elsevier Academic Press.
Gao S-H, Shen L-L, Wen H-Z, Zhao Y-D, Chen P-H, Ruan H-Z (2020) The projections from the anterior cingulate cortex to the nucleus accumbens and ventral tegmental area contribute to neuropathic pain-evoked aversion in rats. Neurobiol Dis 140. https://doi.org/10.1016/j.nbd.2020.104862 104862.
Goffer Y, Xu D, Eberle SE, D'amour J, Lee M, Tukey D, Froemke RC, Ziff EB, Wang J (2013) Calcium-permeable AMPA receptors in the nucleus accumbens regulate depression-like behaviors in the chronic neuropathic pain state. J Neurosci 33:19034–19044. https://doi.org/10.1523/JNEUROSCI.2454-13.2013.
Guo Q, Wang D, He X, Feng Q, Lin R, Xu F, Fu L, Luo M (2015) Whole-brain mapping of inputs to projection neurons and cholinergic interneurons in the dorsal striatum. PLoS One 10:e0123381.
Hintiryan H, Foster NN, Bowman I, Bay M, Song MY, Gou L, Yamashita S, Bienkowski MS, Zingg B, Zhu M, Yang XW, Shih JC, Toga AW, Dong H-W (2016) The mouse cortico-striatal projectome. Nat Neurosci 19:1100–1114. https://doi.org/10.1038/nn.4332.
Hogrefe N, Blom SM, Valentinova K, Ntamati NR, Jonker LJE, Nevian NE, Nevian T (2022) Long-lasting, pathway-specific impairment of a novel form of spike-timing-dependent long-term depression by neuropathic pain in the anterior cingulate cortex. J Neurosci 42:2166–2179. https://doi.org/10.1523/JNEUROSCI.0326-21.2022.
Huang S, Zhang Z, Gambeta E, Xu SC, Thomas C, Godfrey N, Chen L, M'Dahoma S, Borgland SL, Zamponi GW (2020) Dopamine inputs from the ventral tegmental area into the medial prefrontal cortex modulate neuropathic pain-associated behaviors in mice. Cell Rep 31. https://doi.org/10.1016/j.celrep.2020.107812 107812.
Hunnicutt BJ, Jongbloets BC, Birdsong WT, Gertz KJ, Zhong H, Mao T (2016) A comprehensive excitatory input map of the striatum reveals novel functional organization. eLife 5:e19103.
Jankowski MM, Ronnqvist KC, Tsanov M, Vann SD, Wright NF, Erichsen JT, Aggleton JP, O'Mara SM (2013) The anterior thalamus provides a subcortical circuit supporting memory and spatial navigation. Front Syst Neurosci 7. https://doi.org/10.3389/fnsys.2013.00045.
Jercog D, Winke N, Sung K, Fernandez MM, Francioni C, Rajot D, Courtin J, Chaudun F, Jercog PE, Valerio S, Herry C (2021) Dynamical prefrontal population coding during defensive behaviours. Nature 595:690–694. https://doi.org/10.1038/s41586-021-03726-6.
Johannes CB, Le TK, Zhou X, Johnston JA, Dworkin RH (2010) The Prevalence of Chronic Pain in United States Adults: Results of an Internet-Based Survey. J Pain 11:1230–1239. https://doi.org/10.1016/j.jpain.2010.07.002.
Johansen JP, Fields HL (2004) Glutamatergic activation of anterior cingulate cortex produces an aversive teaching signal. Nat Neurosci 7:398–403. https://doi.org/10.1038/nn1207.
Johansen JP, Fields HL, Manning BH (2001) The affective component of pain in rodents: direct evidence for a contribution of the anterior cingulate cortex. Proc Natl Acad Sci 98:8077–8082.
Kasanetz F, Lafourcade M, Deroche-Gamonet V, Revest J-M, Berson N, Balado E, Fiancette J-F, Renault P, Piazza P-V, Manzoni OJ (2013) Prefrontal synaptic markers of cocaine addiction-like behavior in rats. Mol Psychiatry 18:729–737. https://doi.org/10.1038/mp.2012.59.
Kasanetz F, Manzoni OJ (2009) Maturation of Excitatory Synaptic Transmission of the Rat Nucleus Accumbens From Juvenile to Adult. J Neurophysiol 101:2516–2527. https://doi.org/10.1152/jn.91039.2008.
Kasanetz F, Nevian T (2021) Increased burst coding in deep layers of the ventral anterior cingulate cortex during neuropathic pain. Sci Rep 11:24240. https://doi.org/10.1038/s41598-021-03652-7.
Kasanetz F, Riquelme LA, Della-Maggiore V, O'Donnell P, Murer MG (2008) Functional integration across a gradient of corticostriatal channels controls UP state transitions in the dorsal striatum. Proc Natl Acad Sci USA 105:8124–8129. https://doi.org/10.1073/pnas.0711113105.
Koga K, Descalzi G, Chen T, Ko H-G, Lu J, Li S, Son J, Kim T, Kwak C, Huganir RL, Zhao M, Kaang B-K, Collingridge GL, Zhuo M (2015) Coexistence of Two Forms of LTP in ACC Provides a Synaptic Mechanism for the Interactions between Anxiety and Chronic Pain. Neuron 85:377–389. https://doi.org/10.1016/j.neuron.2014.12.021.
Kravitz AV, Freeze BS, Parker PRL, Kay K, Thwin MT, Deisseroth K, Kreitzer AC (2010) Regulation of parkinsonian motor behaviours by optogenetic control of basal ganglia circuitry. Nature 466:622–626. https://doi.org/10.1038/nature09159.
Kravitz AV, Kreitzer AC (2012) Striatal Mechanisms Underlying Movement, Reinforcement, and Punishment. Physiology 27:167–177. https://doi.org/10.1152/physiol.00004.2012.
Kravitz AV, Tye LD, Kreitzer AC (2012) Distinct roles for direct and indirect pathway striatal neurons in reinforcement. Nat Neurosci 15:816–818. https://doi.org/10.1038/nn.3100.
Kuner R, Flor H (2017) Structural plasticity and reorganisation in chronic pain. Nat Rev Neurosci 18:20–30. https://doi.org/10.1038/nrn.2016.162.
LaBuda CJ, Fuchs PN (2000) A Behavioral Test Paradigm to Measure the Aversive Quality of Inflammatory and Neuropathic Pain in Rats. Exp Neurol 163:490–494. https://doi.org/10.1006/exnr.2000.7395.
LaGraize SC, Labuda CJ, Rutledge MA, Jackson RL, Fuchs PN (2004) Differential effect of anterior cingulate cortex lesion on mechanical hypersensitivity and escape/avoidance behavior in an animal model of neuropathic pain. Exp Neurol 188:139–148. https://doi.org/10.1016/j.expneurol.2004.04.003.
Lançon K, Qu C, Navratilova E, Porreca F, Séguéla P (2021) Decreased dopaminergic inhibition of pyramidal neurons in anterior cingulate cortex maintains chronic neuropathic pain. Cell Rep 37. https://doi.org/10.1016/j.celrep.2021.109933 109933.
Lee J-Y, You T, Lee C-H, Im GH, Seo H, Woo C-W, Kim S-G (2022) Role of anterior cingulate cortex inputs to periaqueductal gray for pain avoidance. Curr Biol 32:2834–2847.e5. https://doi.org/10.1016/j.cub.2022.04.090.
Lee M, Manders TR, Eberle SE, Su C, D'amour J, Yang R, Lin HY, Deisseroth K, Froemke RC, Wang J (2015) Activation of corticostriatal circuitry relieves chronic neuropathic pain. J Neurosci 35:5247–5259. https://doi.org/10.1523/JNEUROSCI.3494-14.2015.
Li X-H, Matsuura T, Xue M, Chen Q-Y, Liu R-H, Lu J-S, Shi W, Fan K, Zhou Z, Miao Z, Yang J, Wei S, Wei F, Chen T, Zhuo M (2021) Oxytocin in the anterior cingulate cortex attenuates neuropathic pain and emotional anxiety by inhibiting presynaptic long-term potentiation. Cell Rep 36. https://doi.org/10.1016/j.celrep.2021.109411 109411.
Li X-Y, Ko H-G, Chen T, Descalzi G, Koga K, Wang H, Kim SS, Shang Y, Kwak C, Park S-W, Shim J, Lee K, Collingridge GL, Kaang B-K, Zhuo M (2010) Alleviating neuropathic pain

hypersensitivity by inhibiting PKM in the anterior cingulate cortex. Science 330:1400–1404. https://doi.org/10.1126/science.1191792.

Liu J, Zhang M-Q, Wu X, Lazarus M, Cherasse Y, Yuan M-Y, Huang Z-L, Li R-X (2017) Activation of parvalbumin neurons in the rostrodorsal sector of the thalamic reticular nucleus promotes sensitivity to pain in mice. Neuroscience 366:113–123. https://doi.org/10.1016/j.neuroscience.2017.10.013.

Lobo MK, Covington HE, Chaudhury D, Friedman AK, Sun H, Damez-Werno D, Dietz DM, Zaman S, Koo JW, Kennedy PJ, Mouzon E, Mogri M, Neve RL, Deisseroth K, Han M-H, Nestler EJ (2010) Cell type-specific loss of BDNF signaling mimics optogenetic control of cocaine reward. Science 330:385–390. https://doi.org/10.1126/science.1188472.

Meda KS, Patel T, Braz JM, Malik R, Turner ML, Seifikar H, Basbaum AI, Sohal VS (2019) microcircuit mechanisms through which mediodorsal thalamic input to anterior cingulate cortex exacerbates pain-related aversion S0896627319303319. Neuron. https://doi.org/10.1016/j.neuron.2019.03.042.

Nishio Y, Hashimoto M, Ishii K, Mori E (2011) Neuroanatomy of a neurobehavioral disturbance in the left anterior thalamic infarction. J Neurol Neurosurg Psychiatry 82:1195–1200. https://doi.org/10.1136/jnnp.2010.236463.

Price TJ, Basbaum AI, Bresnahan J, Chambers JF, De Koninck Y, Edwards RR, Ji R-R, Katz J, Kavelaars A, Levine JD, Porter L, Schechter N, Sluka KA, Terman GW, Wager TD, Yaksh TL, Dworkin RH (2018) Transition to chronic pain: opportunities for novel therapeutics. Nat Rev Neurosci. https://doi.org/10.1038/s41583-018-0012-5.

Qi R, Liu C, Weng Y, Xu Q, Chen L, Wang F, Zhang LJ, Lu GM (2016) Disturbed interhemispheric functional connectivity rather than structural connectivity in irritable bowel syndrome. Front Mol Neurosci 9. https://doi.org/10.3389/fnmol.2016.00141.

Reiner A (2010) Corticostriatal projection neurons – dichotomous types and dichotomous functions. Front Neuroanat 4. https://doi.org/10.3389/fnana.2010.00142.

Ren W, Centeno MV, Berger S, Wu Y, Na X, Liu X, Kondapalli J, Apkarian AV, Martina M, Surmeier DJ (2015) The indirect pathway of the nucleus accumbens shell amplifies neuropathic pain. Nat Neurosci 19:220–222. https://doi.org/10.1038/nn.4199.

Ren W, Centeno MV, Wei X, Wickersham I, Martina M, Apkarian AV, Surmeier DJ (2021) Adaptive alterations in the mesoaccumbal network after peripheral nerve injury. Pain 162:895–906. https://doi.org/10.1097/j.pain.0000000000002092.

Santello M, Bisco A, Nevian NE, Lacivita E, Leopoldo M, Nevian T (2017) The brain-penetrant 5-HT7 receptor agonist LP-211 reduces the sensory and affective components of neuropathic pain. Neurobiol Dis 106:214–221. https://doi.org/10.1016/j.nbd.2017.07.005.

Santello M, Nevian T (2015) Dysfunction of cortical dendritic integration in neuropathic pain reversed by serotoninergic neuromodulation. Neuron 86:233–246. https://doi.org/10.1016/j.neuron.2015.03.003.

Schwartz N, Temkin P, Jurado S, Lim BK, Heifets BD, Polepalli JS, Malenka RC (2014) Decreased motivation during chronic pain requires long-term depression in the nucleus accumbens. Science 345:535–542. https://doi.org/10.1126/science.1253994.

Scott DJ, Heitzeg MM, Koeppe RA, Stohler CS, Zubieta J-K (2006) Variations in the human pain stress experience mediated by ventral and dorsal basal ganglia dopamine activity. J Neurosci 26:10789–10795. https://doi.org/10.1523/JNEUROSCI.2577-06.2006.

Sellmeijer J, Mathis V, Hugel S, Li X-H, Song Q, Chen Q-Y, Barthas F, Lutz P-E, Karatas M, Luthi A, Veinante P, Aertsen A, Barrot M, Zhuo M, Yalcin I (2018) Hyperactivity of anterior cingulate cortex areas 24a/24b drives chronic pain-induced anxiodepressive-like consequences. J Neurosci 38:3102–3115. https://doi.org/10.1523/JNEUROSCI.3195-17.2018.

Shepherd GMG (2013) Corticostriatal connectivity and its role in disease. Nat Rev Neurosci 14:278–291. https://doi.org/10.1038/nrn3469.

Tölle TR, Kaufmann T, Siessmeier T, Lautenbacher S, Berthele A, Munz F, Zieglgänsberger W, Willoch F, Schwaiger M, Conrad B, Bartenstein P (1999) Region-specific encoding of sensory and affective components of pain in the human brain: a positron emission tomography correlation analysis. Ann Neurol 45:40–47. https://doi.org/10.1002/1531-8249(199901)45:1 < 40::aid-art8 > 3.0.co;2-l.

Vogt BA, Paxinos G (2014) Cytoarchitecture of mouse and rat cingulate cortex with human homologies. Brain Struct Funct 219:185–192. https://doi.org/10.1007/s00429-012-0493-3.

Watanabe M, Narita M, Hamada Y, Yamashita A, Tamura H, Ikegami D, Kondo T, Shinzato T, Shimizu T, Fukuchi Y, Muto A, Okano H, Yamanaka A, Tawfik VL, Kuzumaki N, Navratilova E, Porreca F, Narita M (2018) Activation of ventral tegmental area dopaminergic neurons reverses pathological allodynia resulting from nerve injury or bone cancer. Mol Pain 14. https://doi.org/10.1177/1744806918756406.

Zhang Q, Manders T, Tong AP, Yang R, Garg A, Martinez E, Zhou H, Dale J, Goyal A, Urien L (2017) Chronic pain induces generalized enhancement of aversion. Elife 6:e25302.

Zhang Y, Liu N, Wang Z, Liu J, Ren M, Hong Y, Luo X, Liu H, Huo J, Wang Z (2022) Impaired Inter-Hemispheric Functional Connectivity during Resting State in Female Patients with Migraine. Brain Sci 12:1505. https://doi.org/10.3390/brainsci12111505.

Zhao R, Zhou H, Huang L, Xie Z, Wang J, Gan W-B, Yang G (2018) Neuropathic Pain Causes Pyramidal Neuronal Hyperactivity in the Anterior Cingulate Cortex. Front Cell Neurosci 12:107. https://doi.org/10.3389/fncel.2018.00107.

Zhou H, Zhang Q, Martinez E, Dale J, Hu S, Zhang E, Liu K, Huang D, Yang G, Chen Z, Wang J (2018) Ketamine reduces aversion in rodent pain models by suppressing hyperactivity of the anterior cingulate cortex. Nat Commun 9. https://doi.org/10.1038/s41467-018-06295-x.

Zhuang X, Huang L, Gu Y, Wang L, Zhang R, Zhang M, Li F, Shi Y, Mo Y, Dai Q, Wei C, Wang J (2019) The anterior cingulate cortex projection to the dorsomedial striatum modulates hyperalgesia in a chronic constriction injury mouse model. Arch Med Sci 17:1388–1399. https://doi.org/10.5114/aoms.2019.85202.

## APPENDIX A. SUPPLEMENTARY DATA

Supplementary data to this article can be found online at https://doi.org/10.1016/j.neuroscience.2023.05.017.

*(Received 21 February 2023, Accepted 18 May 2023)*
*(Available online 24 May 2023)*